GEOPHYSICAL RESEARCH LETTERS, VOL. 36, L09815, doi:10.1029/2009GL037173, 2009

Click Here for Full Article

Radiative effects of upper tropospheric clouds observed by Aura MLS and CloudSat

Hui Su,[1] Jonathan H. Jiang,[1] Graeme L. Stephens,[2] Deborah G. Vane,[1] and Nathaniel J. Livesey[1]

Received 5 January 2009; revised 23 March 2009; accepted 8 April 2009; published 12 May 2009.

[1] The radiative effects of upper tropospheric (UT) clouds observed by CloudSat and Aura MLS during June-July-August 2008 are examined and contrasted. We find that the UT cloud occurrence frequency observed by MLS is more than CloudSat by 4–10% in the tropical average and by 40∼60% near the tropopause in the deep convective regions. The clouds detected by MLS but missed by CloudSat (denoted as TCC) typically have visible optical thickness less than 0.2. TCC produce a tropical-mean net warming of 3.5 W/m^2 at the top-of-atmosphere and net cooling of 1.2 W/m^2 at the surface. They induce a net radiative heating in the UT. Their heating rate at 200 hPa is ∼0.35 K/day in the tropical-mean and ∼0.8 K/day over South Asia, which is about 3–4 times the clear-sky radiative heating rate. Hence, they are potentially important in affecting the mass transport rates from the troposphere to the stratosphere. **Citation:** Su, H., J. H. Jiang, G. L. Stephens, D. G. Vane, and N. J. Livesey (2009), Radiative effects of upper tropospheric clouds observed by Aura MLS and CloudSat, *Geophys. Res. Lett.*, *36*, L09815, doi:10.1029/2009GL037173.

1. Introduction

[2] Clouds cool the Earth by reflecting solar radiation and warm the Earth by trapping thermal emissions. For high-altitude clouds, their longwave (LW) and shortwave (SW) effects can be comparable in magnitude, making their net effect more uncertain than lower-altitude clouds. Thin cirrus clouds tend to have a net warming as their greenhouse effect overcomes their albedo effect, while thick cirrus anvils may tend to have a net cooling [e.g., *Stephens et al.*, 1990; *Ramanathan and Collins*, 1991]. The radiative heating/cooling rate induced by cirrus clouds in the tropical tropopause layer (TTL) has also been considered an important factor in affecting mass transport from the troposphere to the stratosphere [e.g., *Hartmann et al.*, 2001; *Corti et al.*, 2006]. Accurate quantification of cirrus radiative effects relies on accurate measurements of cirrus cloud profiles. This is now possible with the advent of the NASA A-train satellite instruments, in particular, CloudSat, CALIPSO, and Aura Microwave Limb Sounder (MLS).

[3] CloudSat provides a global survey of tropospheric cloud profiles with a nadir-viewing 94 GHz Cloud Profiling Radar. The global cloud liquid and ice water content (L/IWC) profiles are retrieved based on the empirical log-linear relationship between the radar reflectivity (Z_e) and L/IWC when $Z_e > -31$ dBz [*Austin et al.*, 2009; *Wu et al.*, 2009]. Hence, CloudSat cannot detect thin cirrus of small IWC and non-precipitating liquid clouds of small LWC. Aura MLS measures upper tropospheric (UT) ice clouds at ∼11km (215 hPa) and higher using a 240 GHz radiometer [*Wu et al.*, 2008]. It can detect some thin cirrus that is below CloudSat detection limit. The CALIPSO lidar, operating at 532 nm and 1064 nm, can detect even thinner clouds than MLS. *Haladay and Stephens* [2009] (hereinafter referred to as HS09) analyzed joint observations from CloudSat and CALIPSO for June, July, and August (JJA) 2006. They found the thin ice clouds detected by CALIPSO but missed by CloudSat have a cloud cover of ∼25% in the tropics (20°S–20°N). Their optical depth ranged between 0.02–0.3. These thin clouds produced less than 2 W/m^2 shortwave cooling and ∼20 W/m^2 longwave warming at the top-of-atmosphere (TOA) instantaneously, with tropical-mean atmospheric heating of ∼4 W/m^2. In this study, we compare the UT cloud observations from MLS and CloudSat, and perform radiative transfer calculations using these data as inputs. Our aim is to quantify how much more thin cirrus clouds are detected by MLS than by CloudSat and what are the radiative effects of these additional clouds at NOA and the surface, as well as their radiative heating rates in the atmosphere. This study enables users of both data sets to have a quantitative view of the consistency and discrepancy of these measurements, and the advantages and limitations of each instrument.

2. Data Sets

[4] We analyze data during JJA 2008, the same season as in HS09, chosen because the Aura and CloudSat/CALIPSO orbits have been aligned within ∼10 km in terms of equatorial cross position over that period. Prior to May 2008, the Aura MLS track was about 200 km away from the CloudSat/CALIPSO tracks, making a direct comparison of the cloud scenes difficult. The CloudSat IWC/LWC is taken from the Level 2B R04 data set [*Austin et al.*, 2009], with a horizontal resolution of 1.7 km along-track and 1.3 km cross-track. The vertical resolution is ∼500 m. The MLS IWC is from the Level 2 v2.2 product, with a horizontal resolution of ∼200 km along-track and ∼7 km cross-track. The vertical resolution is ∼3 km [*Wu et al.*, 2008]. When comparing the 3-month mean cirrus distributions, we average both CloudSat and MLS data onto the same 8° (longitude) × 4° (latitude) × 3 km (height) grids centered on the MLS standard retrieval levels at 215 hPa (∼11 km), 147 hPa (∼13 km) and 100 hPa (∼16 km). For

[1]Jet Propulsion Laboratory, California Institute of Technology, Pasadena, California, USA.
[2]Department of Atmospheric Science, Colorado State University, Fort Collins, Colorado, USA.

Copyright 2009 by the American Geophysical Union.
0094-8276/09/2009GL037173$05.00

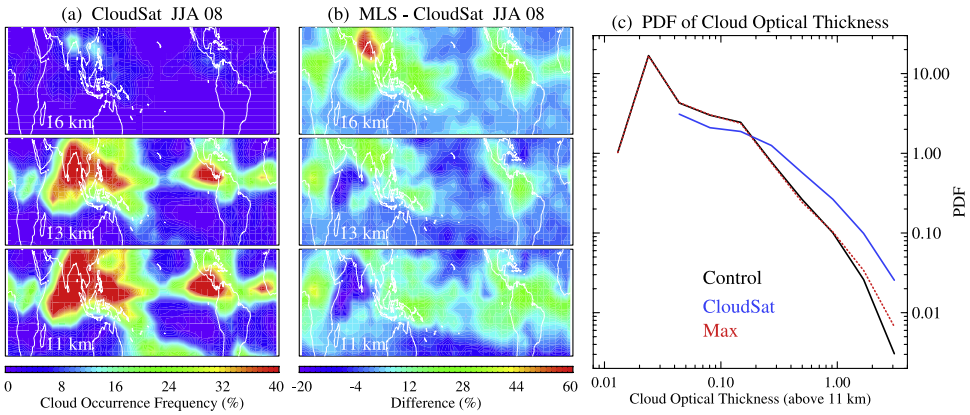

Figure 1. (a) Maps of cloud occurrence frequency at three upper tropospheric levels during June-July-August 2008 from CloudSat, (b) the difference between MLS and CloudSat data, and (c) the probability density function (PDF) of the optical thickness of clouds based at 215 hPa and higher for the "Control", "CloudSat" and "Max" runs.

radiation calculations, we average the CloudSat IWC onto $2^\circ \times 0.2^\circ$ areas centered on the MLS measurement locations (approximately matching the MLS footprints) and run the radiative transfer model along the MLS tracks. Then radiative fluxes and heating rates are gridded onto $8^\circ \times 4^\circ$ boxes for horizontal maps.

[5] The Fu-Liou radiative transfer model is used [*Fu and Liou*, 1993]. For atmospheric temperature, we use the data from Atmospheric Infrared Sounder (AIRS) on Aqua satellite (Level 3, $1^\circ \times 1^\circ$ horizontal resolution) averaged onto the approximate MLS footprints, same as for the CloudSat data. For water vapor, we use AIRS H_2O up to 200 hPa and MLS H_2O above because the AIRS retrieved H_2O degrades in the higher altitudes [*Fetzer et al.*, 2008]. The ozone profile is based on the standard tropical atmosphere. The sea surface temperature (SST) is from the Advanced Microwave Scanning Radiometer (AMSR-E) ($0.25^\circ \times 0.25^\circ$ resolution) on Aqua. For land surface, a constant skin temperature of 300 K is used. The land surface albedo data are taken from the Moderate Resolution Imaging Spectroradiometer (MODIS) Filled Land Surface Albedo Product at 0.3–0.7 μm wavelength. Both SST and albedo are interpolated onto the MLS measurement locations. To evaluate the calculated radiative fluxes, we compare our model results with the JJA mean values from the Clouds and the Earth's Radiant Energy System (CERES) Energy Balanced and Filled (EBAF) 5-year climatology (March 2000 to October 2005) of TOA radiative fluxes [*Wielicki et al.*, 1996] and zonal-mean surface radiative flux estimates based on the International Satellite Cloud Climatology Project (ISCCP) [*Zhang et al.*, 2004] and Global Energy and Water Cycle Experiment-Surface Radiation Budget (GEWEX-SRB) project [*Raschke et al.*, 2006].

3. CloudSat and MLS Observed Cirrus Distributions

[6] We first derive cloud occurrence frequency in the UT during JJA 2008 by dividing the number of cloudy measurements by the number of total measurements in each 8° (longitude) $\times$ 4° (latitude) $\times$ 3 km (height) volume. Figure 1 displays the maps of the 3-month mean cloud occurrence frequency at 11 km, 13 km, and 16 km for CloudSat and the difference between MLS and CloudSat (MLS minus CloudSat) in the tropics (30°S–30°N). At 16 km, MLS produces higher UT cloud occurrence frequency than CloudSat ubiquitously. The large differences mostly occur in the deep convective regions, with a pronounced high occurrence of 40–60% over the South Asia monsoon region. At 13 km, MLS also yields higher cloud occurrence than CloudSat in the convection centers, but MLS underestimates cloud occurrence in certain areas such as the western Indian Ocean, North Pacific and Atlantic, and South Pacific. The MLS underestimate of cloud occurrence is also clear at 11 km. This could be due to the coarse resolution of MLS observations and/or saturation of cloud signal when IWC > 50–120 mg/m^3 (depending on heights) associated with the signal to noise ratio [*Wu et al.*, 2008]. The average difference between MLS and CloudSat cloud occurrence frequency within 30°S–30°N is about 10%, 4% and 6% at 16 km, 13 km and 11 km, respectively. The higher cloud occurrence frequency derived from MLS data reflects the fact that MLS has greater sensitivity to thin clouds than CloudSat. As altitudes increase from 11 km to 16 km, more thin clouds exist so that there is larger difference between the MLS and CloudSat derived occurrence frequency. We abbreviate the thin clouds captured by MLS but missed by CloudSat as TCC.

[7] We also compared the IWC values from MLS and CloudSat for this period. CloudSat and MLS retrieved IWC have similar morphology, but the CloudSat IWC values are generally larger than MLS by a factor of 2 or greater, possibly due to the different cloud particle size assumptions for the IWC retrievals. Our results are similar to those from *Wu et al.* [2009, Figure 6].

[8] We calculated the visible (0.2–0.7 μm) optical thickness (τ) of the UT (pressure $\leq$215 hPa) clouds using the Fu-Liou radiative transfer model with CloudSat and MLS IWC as inputs. The cloud particle size is calculated as a function of the observed IWC and AIRS temperature based on the size distribution parameterization by *McFarquhar and Heymsfield* [1997]. We run the model for three cases. The first case, the "Control" run, uses MLS IWC at 215 hPa and higher altitudes combined with CloudSat L/IWC below 215 hPa. The second case, the "CloudSat" run, uses only CloudSat L/IWC throughout the atmospheric column. The

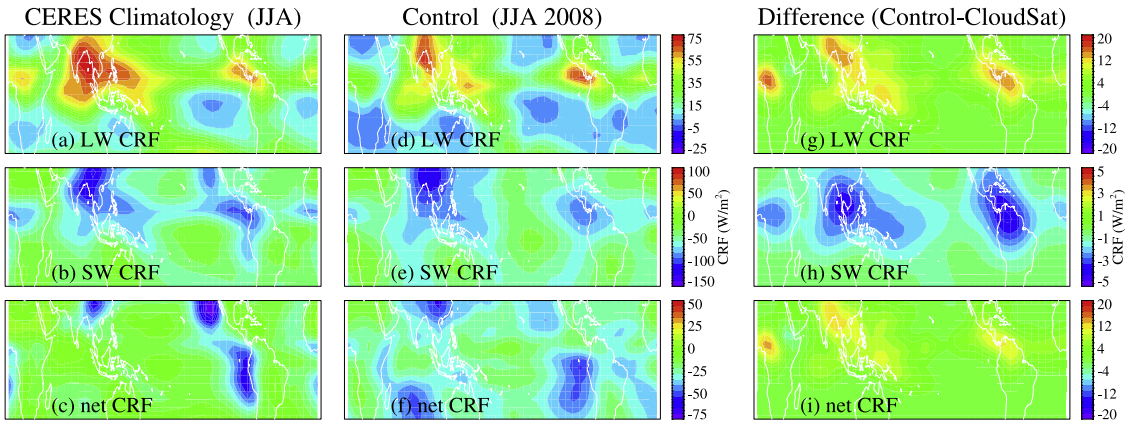

Figure 2. The observed and modeled longwave, shortwave and net cloud radiative forcings at the top-of-atmosphere. (a, b, c) CERES, (d, e, f) the "Control" run and (g, h, i) the difference between the "Control" run and the "CloudSat" run.

third case, the "Max" run, uses the larger value of CloudSat and MLS IWC at the same height. This run attempts to identify the impact of the IWC retrieval bias between CloudSat and MLS. It gives an upper bound of the ice cloud amount when the maximum possible IWC retrievals are used. The probability density functions (PDF) of the calculated τ in the UT for the three cases are shown in Figure 1c. The "Control" run and the "CloudSat" run have substantially different PDFs of τ while the "Max" run is almost identical to the "Control" run except when $\tau > 1$. The optical thickness of TCC ranges from 0.01 to 0.2, with a peak distribution around $\tau = 0.023$. The PDF of τ in the "CloudSat" run peaks around $\tau = 0.04$, below which CloudSat loses sensitivity. The percentage of cloud measurements for $\tau \leq 0.2$ is 71% for the "Control" run, 34% for the "CloudSat" run and 70% for the "Max" run. When $\tau > 0.2$, the "CloudSat" run has a higher PDF than the "Control" run. Compared to HS09, our calculated τ is somewhat smaller than their estimates based on CALIPSO lidar backscatter, partly because we limit the calculations to cloud altitudes above 215 hPa. It may also be due to different cloud particle size assumptions.

4. Cloud Radiative Forcing at TOA and at the Surface

[9] We define cloud radiative forcing (CRF) as the difference between all-sky and clear-sky radiative fluxes at TOA and the surface, with positive sign representing warming the atmosphere or the surface. Three model runs with different UT IWC inputs as described in the previous section are conducted. The "Control" run serves as a baseline experiment and is compared to CERES and ISCCP data in detail for evaluation of the radiative transfer calculations. The differences between the "Control" run and the other two runs thus illustrate the CRFs caused by the different UT IWCs.

[10] Figure 2 shows the TOA LW, SW and net CRF for the CERES JJA climatology, the "Control" run and the difference between the "Control" run and the "CloudSat" run. The results for the "Max" run are very similar to the "Control" run and thus not shown. The tropical-mean (30°S–30°N) CRFs at TOA and the surface for observations and the three model runs are listed in Table 1. For CRF at the surface (SFC), direct observations are difficult and the available "observational" data are either calculated from radiative transfer models using observed atmosphere and cloud profiles as inputs or based on empirical relations between TOA and SFC radiative fluxes. As SFC CRF is not available from CERES EBAF data, we use the tropical-mean TOA and SFC CRF estimates from ISCCP [*Zhang et al.*, 2004] in Table 1 for observations. The ISCCP SFC CRF estimates came from radiative transfer model calculations with the best available atmospheric state variables and ISCCP cloud information as inputs for the period of 1984 to 2004. A rough specification of uncertainties for each term is given according to *Zhang et al.* [2004] and *Raschke et al.* [2006].

[11] In Figure 2, the TOA CRFs in the "Control" run compare fairly well with the CERES climatology, which is regridded from the original 1° × 1° to the same 8° × 4° grids as the model results. Large cloud forcings are found over the convective centers, including Western Pacific, South Asian monsoon region, central Africa and America, and intertropical convergence zone (ITCZ). The modeled LW CRF is somewhat weaker than CERES. This may reflect contributions from even thinner cirrus not captured by MLS. The tropical mean LW CRF at TOA in the "Control" run is 21.7 W/m^2, about 7.5 W/m^2 smaller than that of CERES EBAF 5-year climatology and about 5 W/m^2 smaller than the ISCCP average for 1984–2004 (Table 1). The TOA SW CRF in the "Control" run is similar to CERES in morphology and amplitude. The major deficiency is in the west coast of California, likely due to the underestimate of stratiform clouds by CloudSat there. The tropical-mean SW CRF at TOA is −46.9 W/m^2 in the "Control" run, comparable to CERES EBAF, −44.0 W/m^2, and ISCCP, −48.0 W/m^2 (Table 1). The net CRF at TOA for the "Control" run is in the ballpark of CERES and ISCCP climatology.

[12] At the surface, the tropical-mean LW warming in the "Control" run is smaller than the ISCCP estimate by ~10 W/m^2. The modeled SFC SW cooling is similar to the ISCCP estimate. Thus, the net SFC CRF in the "Control" run shows a larger net cooling than ISCCP. We conducted three sensitivity runs to test if the specification of land surface temperature, cloud particle size or cloud retrieval bias could cause the large discrepancy between the modeled and ISCCP SFC LW CRF. We found that increasing the

Table 1. Observed and Modeled Tropical Mean Cloud Radiative Forcing at the Top of Atmosphere and at the Surface[a]

	Observations	Control Run of MLS Plus CloudSat	CloudSat Only	Maximum of MLS/CloudSat
TOA-LW	26.6 ± 5.0	21.7	17.0	22.8
TOA-SW	−48.0 ± 5.0	−46.9	−45.7	−47.7
TOA-net	−21.4 ± 10.0	−25.2	−28.7	−24.9
SFC-LW	18.9 ± 10.0	8.3	8.2	8.4
SFC-SW	−50.0 ± 10.0	−51.6	−50.3	−52.6
SFC-net	−31.1 ± 20.0	−43.3	−42.1	−44.2

[a]Observed data are based on ISCCP FD-MPF; the tropical mean is 30°S–30°N. TOA is top of the atmosphere and SFC is at the surface; radiative forcing is given in W/m^2. The ISCCP data are June-July-August (JJA) averages from 1984 to 2004, with rough error estimates from *Zhang et al.* [2004] and *Raschke et al.* [2006] for the ISCCP and GEWEX-SRB projects. The modeled results are for JJA 2008.

land surface temperature from 300 K to 302 K increased the SFC LW CRF by only 0.1 W m^{-2}, while reducing cloud particle size by 50% or doubling the IWC and LWC values increased SFC LW CRF by ~0.6 W m^{-2} and undesirably increased TOA and SFC SW CRF by ~10 W m^{-2} or more. Therefore, it is still not clear what causes the ~10 W m^{-2} discrepancy in SFC LW CRF, and future work is needed to resolve the issue. On the other hand, we note that the discrepancy is comparable to the uncertainty of the ISCCP surface flux estimate.

[13] Given the reasonable comparison between the "Control" run and the CERES and ISCCP data, we focus our attention on the differences of CRFs between the "Control" run and the "CloudSat" run. Shown in Figures 2g, 2h, 2i, the difference between the "Control" and "CloudSat" runs is up to 20 W/m^2 for TOA LW CRF and within 5 W/m^2 for TOA SW CRF in the deep convective regions. Hence, complementing CloudSat IWC measurements with MLS IWC would increase TOA net warming by ~15 W/m^2 in the deep convective regions, resulting in an increase of tropical-mean net warming of 3.5 W/m^2 (4.7 W/m^2 LW warming and −1.2 W/m^2 SW cooling). However, TCC have a relatively weak impact on the surface radiative energy budget. The tropical-mean SFC LW and SW CRF differences between the two runs are 0.1 and −1.3 W/m^2, respectively, resulting in −1.2 W/m^2 net cooling (Table 1).

[14] In the "Max" run, the TOA and SFC CRFs are quite similar to the "Control" run, with a small difference less than 1 W/m^2. This is not surprising as indicated by the comparison of τ in Figure 1c. It suggests that the missed detection of thin cirrus (evaluated by "Control" – "CloudSat") has a larger impact on the TOA cloud forcing than the difference in the IWC values retrieved by CloudSat and MLS (evaluated by "Control" – "Max").

5. Cloud-Induced Radiative Heating Rate

[15] Figure 3 shows the cloud-induced radiative heating rate (CHR, all-sky minus clear-sky heating rates) from the three runs averaged over the tropics (30°S–30°N) and the South Asia monsoon region (10°S–30°N, 60°E–150°E). The tropical-mean CHR is positive over most of the troposphere, except in the boundary layer between 900 and 800 hPa. There is also small cooling in the lower stratosphere due to the LW emission from the cold cloud tops. Between 200 hPa and 100 hPa, there is a marked enhancement of cloud radiative heating when combined MLS and CloudSat IWC are used compared to CloudSat IWC used alone. This heating is largely due to the absorption of solar radiation by cirrus. The tropical-mean CHR at 200 hPa is about 0.15, 0.5 and 0.65 K/day in the "CloudSat", "Control" and "Max" runs, respectively. Over the South Asia monsoon region, the averaged CHR is much larger in the "Control" and "Max" runs than in the "CloudSat" run, owing to the substantially higher TCC occurrence frequency there (Figure 1b). The radiative heating rate at 200 hPa produced by TCC (indicated by the difference between the "Control" run and the "CloudSat" run) is about 0.8 K/day, which is 3–4 times the clear-sky radiative heating rate. As *Corti et al.* [2006] suggested, the larger radiative heating inside the cirrus may provide a faster mass transport pathway for the tracer transport from the troposphere to the stratosphere.

6. Conclusions

[16] This study examines the radiative properties of UT clouds observed by CloudSat and MLS, and compares the TOA and surface cloud forcings and cloud-induced radiative heating rates when different IWC measurements are used. We focus on the effects of the thin cirrus clouds detected by MLS but missed by CloudSat, the TCC. During JJA 2008, the cloud occurrence reported by CloudSat is about 10% less than MLS near the tropopause in the tropical average and is about 60% lower in the South Asia monsoon

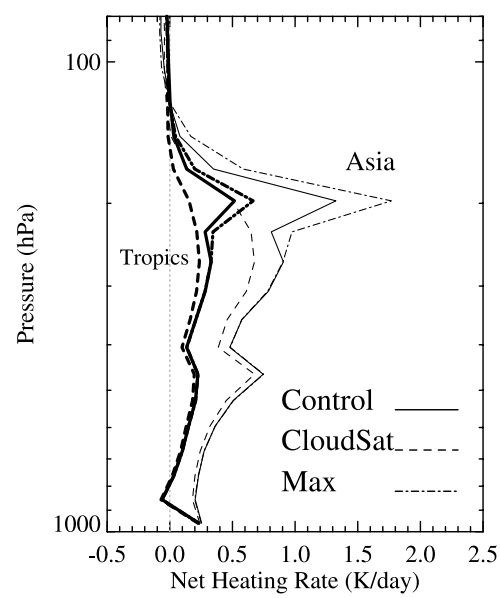

Figure 3. Cloud radiative heating rates in the atmosphere averaged over the tropics (thicker lines) and the South Asia region (thinner lines) for the three runs. The dotted line corresponds to zero net radiative heating rate.

region. These thin cirrus clouds mostly have optical depth ranging from 0.01 to 0.2. Our radiative transfer calculations show that TCC have a dominantly LW warming effect at TOA. Locally, their LW warming effect at TOA can be as large as 20 W/m^2. On tropical average, they contribute to 3.5 W/m^2 net warming at TOA and −1.2 W/m^2 net cooling at the surface. Our results are consistent with HS09 which estimated the cloud forcings of thin cirrus missed by CloudSat but detected by CALIPSO.

[17] Furthermore, we show that TCC produce a substantial radiative heating in the UT and TTL. Over the South Asia monsoon region, where TCC occur most frequently, their radiative heating rate can be a few times larger than the clear-sky radiative heating rate. Hence, the thin cirrus may be potentially important in altering the vertical transport rates for TTL tracers entering the stratosphere.

[18] This study demonstrates the importance and benefits of merging multiple satellite cloud measurements for accurate assessment of cloud radiative effects. Combining CloudSat and MLS IWC measurements clearly yields better estimates of cloud forcing and cloud radiative heating rates than using CloudSat data alone. However, we recognize that there may remain some thin cirrus missed by CloudSat and MLS combined together. This may be compensated by synthesizing CALIPSO data with CloudSat and MLS. Future work using the three instruments together would hopefully yield a more complete picture of clouds and their radiative effects.

[19] **Acknowledgments.** We thank the funding support from the JPL R&TD and NASA ROSES ACMAP-AST program. We thank Tristan L'Ecuyer for help with CloudSat data, Yu Gu for help with the Fu-Liou radiative transfer modeling, and two anonymous reviewers for helpful comments. This work is conducted at the Jet Propulsion Laboratory, California Institute of Technology, under contract with NASA.

References

Austin, R. T., A. J. Heymsfield, and G. L. Stephens (2009), Retrieval of ice cloud microphysical parameters using the CloudSat millimeter-wave radar and temperature, *J. Geophys. Res.*, *114*, D00A23, doi:10.1029/2008JD010049.

Corti, T., B. P. Luo, Q. Fu, H. Vomel, and T. Peter (2006), The impact of cirrus clouds on tropical troposphere to stratosphere transport, *Atmos. Chem. Phys.*, *6*, 2539–2547.

Fetzer, E. J., et al. (2008), Comparison of upper tropospheric water vapor observations from the Microwave Limb Sounder and Atmospheric Infrared Sounder, *J. Geophys. Res.*, *113*, D22110, doi:10.1029/2008JD010000.

Fu, Q., and K. N. Liou (1993), Parameterization of the radiative properties of cirrus clouds, *J. Atmos. Sci.*, *50*, 2008–2025.

Haladay, T., and G. Stephens (2009), Characteristics of tropical thin cirrus clouds deduced from joint CloudSat and CALIPSO observations, *J. Geophys. Res.*, doi:10.1029/2008JD010675, in press.

Hartmann, D. L., J. R. Holton, and Q. Fu (2001), The heat balance of the tropical tropopause, cirrus, and stratospheric dehydration, *Geophys. Res. Lett.*, *28*(10), 1969–1972.

McFarquhar, G. M., and A. J. Heymsfield (1997), Parameterization of tropical cirrus ice crystal size distributions and implications radiative transfer: Results from CEPEX, *J. Atmos. Sci.*, *54*, 2187–2200.

Ramanathan, V., and W. Collins (1991), Thermodynamics regulation of ocean warming by cirrus clouds deduced from observations of the 1987 El Nino, *Nature*, *351*, 27–32.

Raschke, E., S. Bakan, and S. Kinne (2006), An assessment of radiation budget data provided by the ISCCP and GEWEX-SRB, *Geophys. Res. Lett.*, *33*, L07812, doi:10.1029/2005GL025503.

Stephens, G. L., S. C. Tsay, P. W. Stackhouse, and P. J. Flatau (1990), The relevance of the microphysical and radiative properties of cirrus clouds to climate and climatic feedback, *J. Atmos. Sci.*, *47*, 1742–1754.

Wielicki, B. A., et al. (1996), Clouds and the Earth's Radiant Energy System (CERES): An Earth observing system experiment, *Bull. Am. Meteorol. Soc.*, *77*, 853–868.

Wu, D. L., et al. (2008), Validation of the Aura MLS cloud ice water content (IWC) measurements, *J. Geophys. Res.*, *113*, D15S10, doi:10.1029/2007JD008931.

Wu, D. L., et al. (2009), Comparisons of global cloud ice from MLS, CloudSat, and correlative data sets, *J. Geophys. Res.*, *114*, D00A24, doi:10.1029/2008JD009946.

Zhang, Y., W. B. Rossow, A. A. Lacis, V. Oinas, and M. I. Mishchenko (2004), Calculation of radiative fluxes from the surface to top of atmosphere based on ISCCP and other global data sets: Refinements of the radiative transfer model and the input data, *J. Geophys. Res.*, *109*, D19105, doi:10.1029/2003JD004457.

J. H. Jiang, N. J. Livesey, H. Su, and D. G. Vane, Jet Propulsion Laboratory, California Institute of Technology, Pasadena, CA 91109, USA. (hui.su@jpl.nasa.gov)

G. L. Stephens, Department of Atmospheric Science, Colorado State University, Fort Collins, CO 80523, USA.